

# Pump-turbine Rotor-Stator Interactions in Generating Mode: Pressure Fluctuation in Distributor Channel

EPFL

Ecole polytechnique fédérale de Lausanne  
Switzerland

**Alireza ZOBELI**  
**Jean-Louis KUENY**  
**Mohamed FARHAT**  
**François AVELLAN**

alireza.zobeiri@epfl.ch  
jean-louis.kueny@epfl.ch  
mohamed.farhat@epfl.ch  
francois.avellan@epfl.ch

## Abstract

Investigation of the rotor-stator interactions of a reduced-scale model  $\nu = 0.19$  pump-turbine in generating mode is presented for the maximum discharge operating condition. This operating point is chosen in order to have the most important rotor-stator interactions. The numerical simulation of the unsteady flow is performed with CFX 5.7<sup>TM</sup> for a computing domain which is extended to the full pump-turbine from the spiral casing to the draft tube. A computing domain embracing the full geometry enables to minimize the errors, streaming focus the boundary conditions, the periodic interface or the pitch ratio of rotor-stator interface. It also allows considering the fully non uniformity of the in coming flow field from the spiral casing. The pressure measurements are performed with piezoresistive miniature pressure sensors located in the distributor channels. The pressure fluctuations for one distributor channel obtained from the numerical simulation present a very good agreement with experimental data. The numerical result analysis shows, how the pressure fluctuations at blade passage frequency (BPF) and its harmonics vary along a distributor channel of the pump-turbine. The maximum pressure amplitude of BPF occurs in the rotor-stator zone, but it decreases very fast backward to the stay vane. However, the pressure amplitude of the first harmonic corresponding to 2 times the blade passage frequency spreads to the spiral casing highlighting the -2 precessing diametrical mode resulting from the modulation of the interacting stationary and rotating flow field.

## Résumé

Une étude numérique et expérimentale des interactions rotor-stator présentes dans un modèle réduit de pompe-turbine de vitesse spécifique  $\nu = 0.19$  est proposée en mode turbine. Le calcul instationnaire de l'écoulement est mené dans la machine complète, de la bache spirale jusqu'à l'aspirateur. Le domaine de calcul correspondant permet de minimiser des effets liés aux conditions aux limites ou aux interfaces périodiques. La simulation numérique est réalisée à l'aide du logiciel CFX 5.7<sup>TM</sup>. Les résultats des calculs sont comparés aux mesures de pressions instationnaires; les mesures étant réalisées dans plusieurs canaux du distributeur avec de capteurs piézorésistifs. La comparaison entre les résultats des simulations numériques et les ceux des mesures est excellente. Les résultats mettent en évidence l'évolution dans les canaux du distributeur de la composante fondamentale des fluctuations de pression à la fréquence de passage des aubes et de ses harmoniques. Les amplitudes de la composante fondamentale à la fréquence du passage des aubes de la roue prédominent dans la zone d'interaction mais diminuent très rapidement en remontant vers les entretoises et la bache spirale. Par contre, l'amplitude correspondant à la 1<sup>ère</sup> harmonique des fluctuations de pression, soit 2 fois la fréquence de passage des aubes, se propage jusqu'à la bache spirale, mettant en évidence la précession -2 du mode diamétral résultant de la modulation du champ d'écoulement stationnaire interagissant avec le champ tournant.

## Introduction

Interactions between impeller blade and guide vanes are one of the main causes of vibration in pump-turbines (Ref 13) or blade cracking (Ref 14). The phenomenology of rotor-stator interactions may be considered as a combination of inviscid flow, potential, and viscous flow, wake, interactions (Ref 1). With respect to the potential effect, the flow in the distributor channels is periodically perturbed by the rotating impeller blades. It is one of the main sources of pressure fluctuation extending backward up to the spiral casing. In such a case, Giesing (Ref 2, Ref 3) developed an exact solution for unsteady potential flow. The key operating parameter for potential interaction is the guide vanes impeller blade clearance gap which controls the intensity of the rotor-stator interactions. Therefore, the most important potential interaction will arise for full opening of the guide vanes as shown Figure 1 when one of the impeller blades is in the closest position to a guide vane trailing edge.

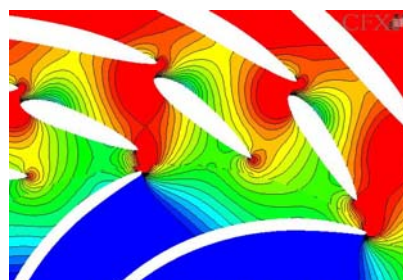


**Figure 1** Field of pressure in the case of the strongest potential interaction.

With respect to the viscous effects, the hydrodynamic phenomena, which play a major role in rotor-stator interactions are non-uniformity of the velocity field in the spiral casing, non desirable flow angle in the distributor, flow separations (Ref 4) and wakes (Ref 5, Ref 6).

The conceptual separation between potential and viscous effects has limitations that modern computational flow dynamics can overcome by enabling unsteady rotor-stator simulations. If we put in perspective the complexity of the different rotor-stator interaction models from the simplest up to fully transient Navier Stokes models with the corresponding computing power required, see Figure 2 (Ref 7), we see that today, the available computing resources enable to resolve 3D RANS equations with transient rotor-stator model.

However, the limitations of the turbulence model in use for such numerical simulations and incompressible flow assumption lead us to carefully investigate these interactions by performing unsteady numerical simulations in the case of a pump-turbine in generating mode and compare to the corresponding experimental results. The investigations are carried out within the EUREKA initiative, HYDRODYNA Project n° 3246 the pan-European framework for research and development cooperation, (Ref 8). In the following paper, the case study is first briefly presented and the experimental conditions introduced. Then, the numerical simulations are presented and the results compared to the measurements. Finally the analysis of the results is provided.

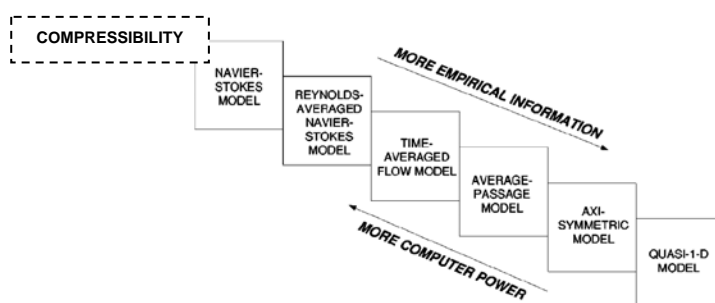


**Figure 2** Rotor-stator numerical models from (Ref 7)

## Case Study and experimental setup

The case study is a reduced scale model of a  $\nu = 0.19$  specific speed pump-turbine, featuring 20 stay vanes, 20 guide vanes and 9 impeller blades see Figure 3. One operating point ( $\varphi = 0.519$ ,  $\psi = 5.254$ ,  $Q = 1.43 Q_{BEP}$ ) is investigated corresponding to the maximum guide vane opening and the minimum clearance of the rotor-stator gap. As usual, the measurements of discharge, specific energy and efficiency are performed in compliance with the requirements of the IEC 60193 standards (Ref 9), the reduced-scale model being installed on the EPFL PF3 test rig.

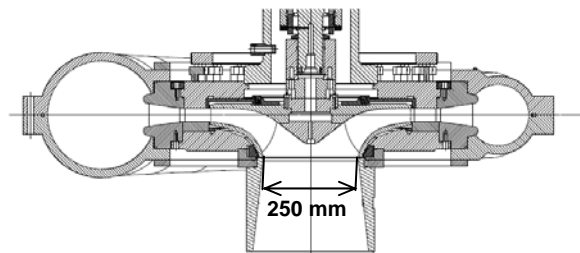


**Figure 3 HYDRODYNA pump-turbine cross-section**

The wall pressure fluctuation measurements are performed on the stationary parts of the pump-turbine model. 48 miniature piezoresistive pressure sensors are mounted on the stay vane and guide vane channels. Both static and dynamic calibrations of the pressure sensors are performed. The dynamic calibration of the pressure transducers is carried out in a large vessel with the help of the EPFL spark generated bubble system (Ref 10) by comparison with a reference piezoelectric pressure sensor. The pressure sensors are mounted in such a way to cover the rotor-stator interaction zone as well as the guide vane and wicket gate channels. 4'200 data samples per impeller rotation during 750 impeller revolutions are measured. The recorded pressure fluctuations are phase-averaged, estimated with the help of a tachymeter signal, allow for a comparison with the numerical simulations. It should be mentioned that experimental data are decimated to match the numerical simulation time step.

## Expected rotor-stator behavior in Francis pump-turbine

In the stator frame, the non uniform flow field at the guide vane outlet caused by wake effect and blade loading generates a periodic flow pattern. In the rotor frame as well, the pressure field attached to the rotating impeller blade induces periodic flow field distortions. These stationary and rotating periodic flows can be expressed as the following Fourier series:

$$p_s(\theta_s, t) = \sum_{n=1}^{\infty} B_n \cos(n \cdot z_o \cdot \theta_s + \phi_n) \quad \text{and} \quad p_r(\theta_r, t) = \sum_{m=1}^{\infty} B_m \cos(n \cdot z_b \cdot \theta_r + \phi_m) \quad (1)$$

Where  $m$ ,  $n$  are the harmonic orders,  $B_m$ ,  $\phi_m$  being respectively the amplitude and the phase for the  $m^{\text{th}}$  harmonic,  $\theta_r$ ,  $\theta_s$  being the angle coordinates for respectively the rotating and the stationary systems,  $z_b$  is the impeller blade number, and  $z_o$  is the guide vanes number.

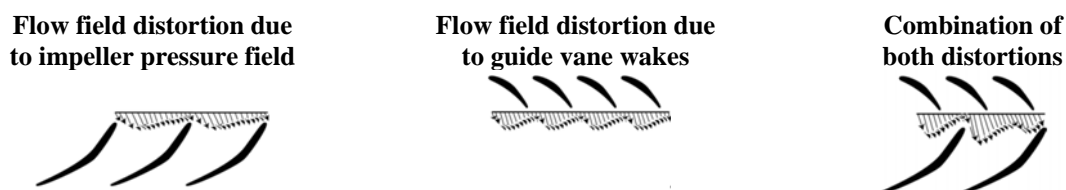


**Figure 4 Modulation process between impeller blade flow and guide vanes flow field**

The resulting pressure field, combining the guide vanes and the impeller blade pressure field is characterized by a strong modulation process as illustrated in Figure 4, (Ref 11, Ref 12). Therefore this modulation can be express as the product of both pressure fields given by equations (1) and, according to the impeller angle coordinate expression for the stationary reference frame,  $\theta_r = \theta_s - \omega t$ , the modulation yields the following resulting pressure field:

$$p_{mn}(\theta_s, t) = \frac{A_{mn}}{2} \cos(m \cdot z_b \cdot \omega t - (m \cdot z_b - n \cdot z_o)\theta_s + \phi_n - \phi_m) + \frac{A_{mn}}{2} \cos(m \cdot z_b \cdot \omega t - (m \cdot z_b + n \cdot z_o)\theta_s + \phi_n - \phi_m) \quad (2)$$

The modulated pressure field results from the contribution of high and low orders diametrical pressure modes,  $k_1$  and  $k_2$ :

$$k_1 = m \cdot z_b - n \cdot z_o \text{ and } k_2 = m \cdot z_b + n \cdot z_o \quad (3)$$

The sign of the diametrical mode number  $k$  indicates the rotating direction of diametrical mode, positive  $k$  value meaning a rotational mode in the same direction than that of the impeller. We have sorted Table 1 the lowest order values for both  $k_1$  and  $k_2$  which should correspond to the highest energy for the diametrical modes. In the present case, the lowest absolute value corresponds to  $k_1 = -2$ ,  $m = 2$  and  $n = 1$ . Therefore, this rather straight forward analysis leads us to expect pressure fluctuations resulting from modulations of rotor stator interactions occurring at 2 times the impeller blade passage frequency in the stationary system,  $f_s/f_b = m \cdot z_b = 18$ , where  $f_b$  is the impeller rotating frequency.

**Table 1. Expected rotor-stator diametrical modes**

$n$	$m$	$k_1 = m \cdot z_b - n \cdot z_o$	$k_2 = m \cdot z_b + n \cdot z_o$	$f_s/f_b = m \cdot z_b$
1	2	-2	38	18
1	3	7	47	27
2	4	-4	76	36
2	5	5	85	45

## Rotor-Stator Numerical Simulation

The computing domain corresponds to the full pump-turbine water passages, from spiral casing down to the draft tube, see Figure 5. This computing domain enables to overcome the influence of boundary conditions, periodic interfaces, pitch ratio of rotor-stator interface and to fully consider the non uniform flow field incoming from the spiral casing.



**Figure 5 Computing domain**

Structured meshes are used in spiral casing. At the end of the spiral casing close to the tongue, unstructured tetrahedral meshes are applied for a better refinement of the spatial discretization. Stay vane and guide vane channels are meshed as a whole. The fore mentioned components are connected to each other by fluid to fluid interfaces. Structured meshes are

used for the rotating domain as well. In the interacting zone between stationary and rotating parts, a mesh refinement is performed in both parts for improving the capture of the unsteady flow features. The mesh characteristics for each component are summarized Table 2. A general view of the structured and unstructured meshes on a plane perpendicular to the axis of rotation is given in Figure 6. The whole mesh generation process is carried out with the help of the ICEMCFD5 software.

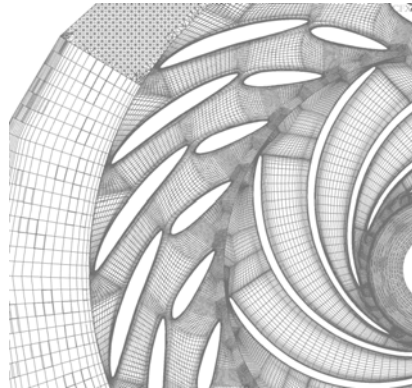


**Figure 6 Mesh in the spiral casing, distributor channels and impeller**

**Table 2. Mesh characteristics of the computing domain**

Components	Nodes per Channel	Minimum Angle	Mean $y^+$	Mesh Software	Mesh Topology
Spiral casing	300,000	23°	120	ICEMCFD 5	Structured
Stay Vanes	60,000	35°	100		
Guide Vanes					
Impeller	150,000	39°	60		
Draft tube	400,000	41°	270		

The unsteady RANS simulations are performed with  $k - \varepsilon$  turbulence model implemented in the CFX-5.7 code. The code is able to solve full transient rotor-stator conditions. The discretization scheme is of second order and the time step corresponds to  $0.5^\circ$  of the impeller rotation. Numerical convergence is set to a maximum of  $10^{-3}$  and periodicity solution is fulfilled after three impeller revolutions. The types of boundary conditions are summarized Table 3 .

**Table 3. Boundary conditions**

B.C	Location	Option
Inlet	Spiral casing inlet	Velocity Profile
Outlet	Draft tube outlet	Const. Average Static pressure
Wall	Solid surfaces	Log. Law

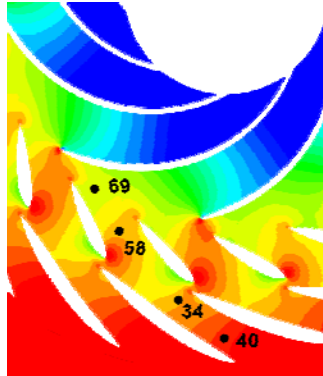
### Comparison of the experimental and numerical results

The numerical results are compared with the experimental data at the locations of the pressure taps in one distributor channel as shown in; i.e. 2 locations on a guide vane and 2 locations in a stay vanes channel. Experimental phase-averaged data and numerical results of one impeller

revolution are analyzed by Fourier transform to obtain the amplitudes of the harmonic components. The pressure coefficient fluctuation is defined below:

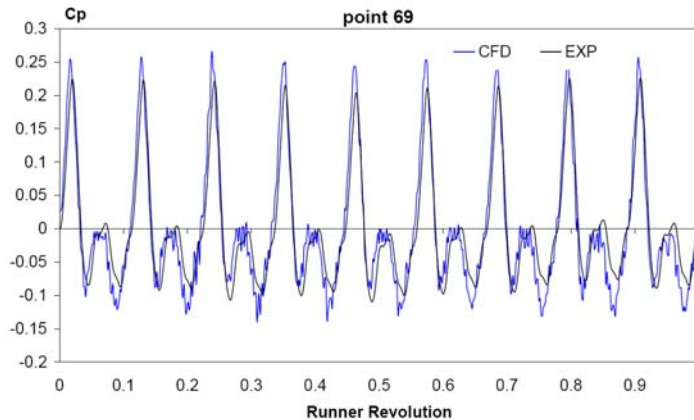
$$c_p = \frac{p - \bar{p}}{\frac{1}{2} \rho \cdot U^2} \quad (4)$$

where  $p$  is the pressure,  $\bar{p}$  the average pressure for one impeller revolution and  $U$  is the impeller peripheral velocity.

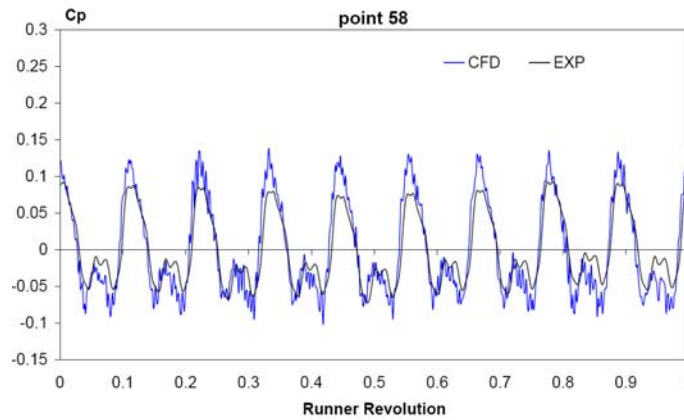


**Figure 7** Locations of the monitoring points in the distributor channel

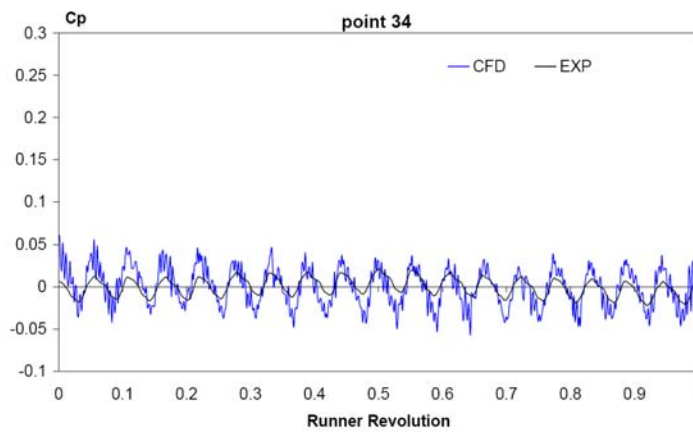
The pressure fluctuations for one impeller revolution are presented Figure 8, Figure 9, Figure 10 and Figure 11. The agreement between measured and computed values is very good. The most significant discrepancy of pressure amplitude arises in the guide vane channel, point 58, see Figure 9. A spectral analysis at the corresponding point highlights that the difference stems from the pressure amplitude value at the impeller blade passing frequency.



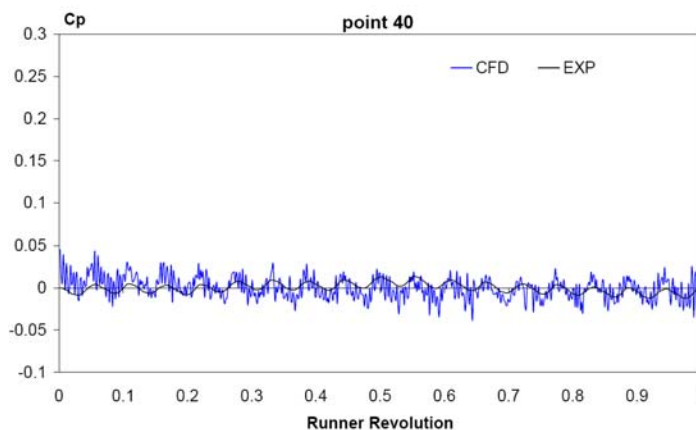
**Figure 8** Time history oscillations of pressure coefficient, comparison between numerical and experimental results at monitoring point 69



**Figure 9** Time history oscillations of pressure coefficient, comparison between numerical and experimental results at monitoring point 58



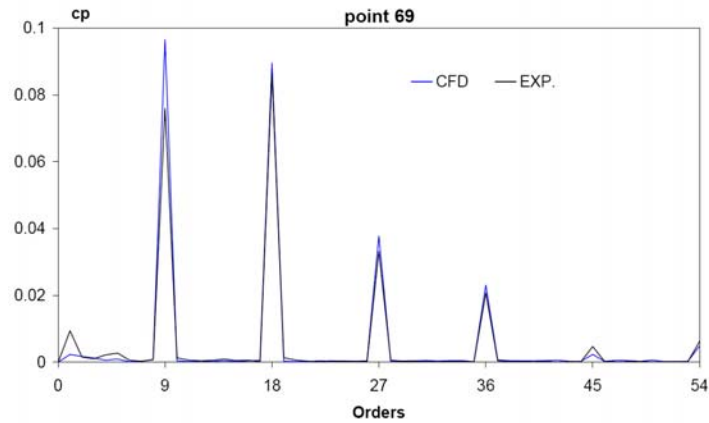
**Figure 10** Time history oscillations of pressure coefficient, comparison between numerical and experimental results at monitoring point 34



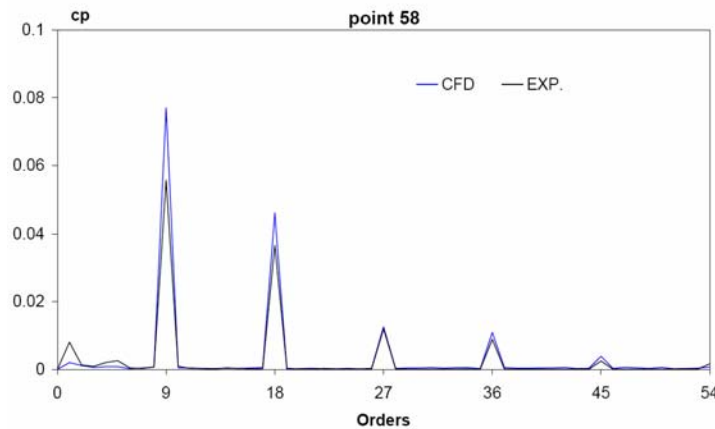
**Figure 11** Time history oscillations of pressure coefficient, comparison between numerical and experimental results at monitoring point 40

Figure 12 to Figure 15 present the frequency spectra of the pressure coefficient at the already mentioned points. The pressure amplitudes corresponding to the blade passing frequency and its harmonics are clearly evidenced by the numerical simulation. For the point 69, the numerical simulations over estimates the amplitude of the blade passing frequency component

by 15% with respect to the experimental results; while for the harmonic components, the pressure amplitude shows a good agreement with the measurements.



**Figure 12** Frequency spectra of pressure coefficient, comparison between numerical and experimental results at monitoring point 69



**Figure 13** Frequency spectra of pressure coefficient, comparison between numerical and experimental results at monitoring point 58

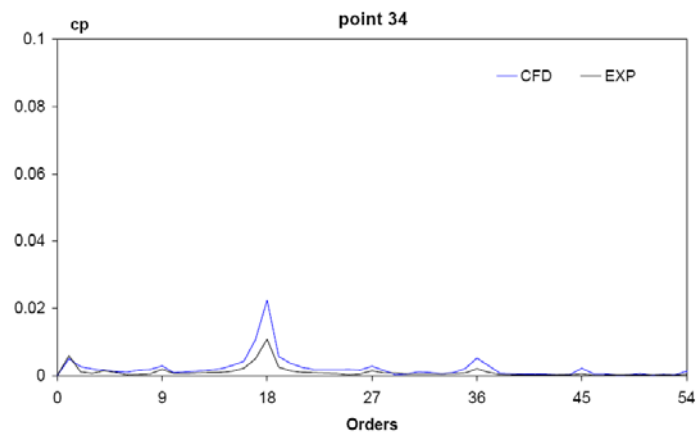


**Figure 14** Frequency spectra of pressure coefficient, comparison between numerical and experimental results at point 34

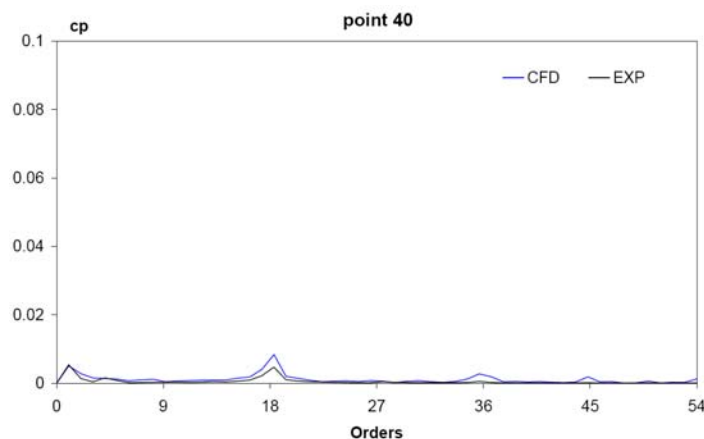


**Figure 15** Frequency spectra of pressure coefficient, comparison between numerical and experimental results at monitoring point 40

### Propagation of the pressure fluctuations in the distributor channel

Figure 16 displays the frequency spectra of the numerical results in the distributor channel (points 40 to 69). The pressure amplitude variation for each point is presented by the dashed lines. The blade passage frequency ( $f_s/f_b = 9$ ) has the maximum amplitude value in the guide vanes (point 69, point 58) while it decreases very fast in the stay vanes (point 34, point 40). The first harmonic pressure fluctuation corresponding to the dominating frequency ( $f_s/f_b = 18$ ,  $k = -2$ ) spreads up to the spiral casing. For point 69, the pressure amplitude at this frequency has almost the same magnitude than that of the impeller blade passage frequency. The other higher harmonics also vanish in the stay vanes channel.

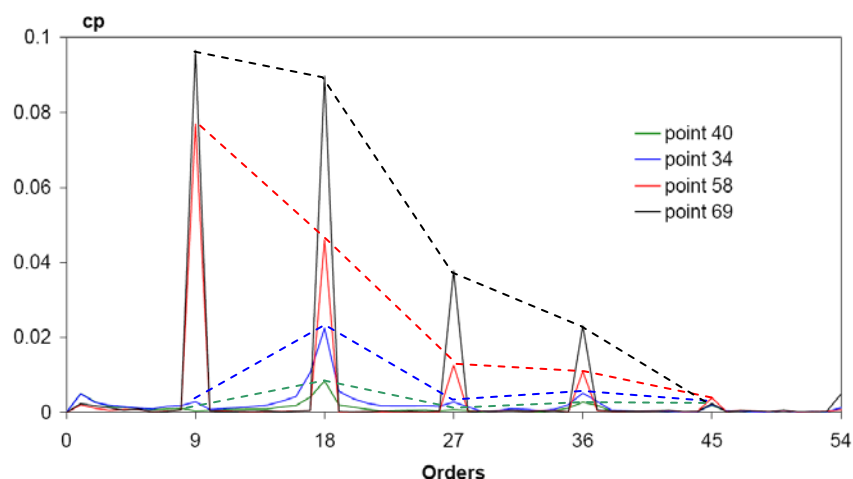


**Figure 16** Frequency components of pressure coefficient in the distributor

### Conclusion

The rotor stator interactions have been investigated in the case of a reduced-scale model of a  $\nu = 0.19$  specific speed pump-turbine, featuring 20 stay vanes, 20 guide vanes and 9 impeller blades. The studied operating point of interest corresponds to the maximum guide vane opening enabling to achieve a minimum clearance for the rotor-stator gap. The unsteady RANS simulations performed with  $k - \varepsilon$  turbulence model implemented in CFX-5.7 code are validated satisfactorily with wall pressure measurements performed in the distributor flow channels. The spectral analysis carried out for the corresponding region highlights that the difference stems from the pressure amplitude value of the blade passage frequency

component. For the point closest to the impeller, the maximum of pressure amplitude is observed for the same component, indicating the strong influence of the potential effect in the interactions between the guide vanes and the rotating impeller blades. However, the amplitude of this component decreases very fast backward to the stay vane. While the 1<sup>st</sup> harmonic corresponding to 2 times blade passage frequency spreads to the spiral casing highlighting the influence of a -2 precessing diametrical mode as predicted by the modulation study of the interacting frequencies; the higher harmonics being cancelled out.

## Acknowledgments

The investigation reported in this paper is part of the work carried out for the HYDRODYNA, Eureka Research Project n° 3246, whose partners are: ALSTOM Hydro, EDF-CIH, EPFL, GE Hydro, UPC-CDIF, VATECH Hydro and VOITH-SIEMENS Hydro Power Generation. The project is also financially supported by CTI the Swiss Federal Commission for Technology and Innovation, grant CTI n° 7045-1. The authors are very grateful to the HYDRODYNA Technical Committee for its involvement and constant support to the project. Finally the staff of the EPFL Laboratory for Hydraulic Machines should be thanked for its support in the experimental and numerical work.

## References

- Ref 1 R.P. Dring, H.D. Joslyn, L.W. Hardin, J. H. Wagner, "Turbine Rotor-Stator Interactions", *Journal of Engineering for Power*, Oct. 1982, Vol. 104, pp 729-742.
- Ref 2 J.P. Giesing, "Nonlinear Two-Dimensional Unsteady Potential Flow with Life" *J. Aircraft*, Mar. – Apr. 1968, Vol. 5, No. 2, pp. 135-143
- Ref 3 J.P. Giesing, "Nonlinear Interaction of two Lifting Bodies in Arbitrary Unsteady Motion", *ASME Journal of Basic Eng.*, Sept. 1968, pp. 387-394
- Ref 4 P.F. Bert, J.F. Combes, J.L. Kueny, "Unsteady flow calculation in a centrifugal pump using a finite element method ", XVIII IAHR Symp., Valencia, Spain, Sept. 1996.
- Ref 5 B. Lakshminarayana, R. Davino, "Mean Velocity and Decay Characteristics of the Guidevane and Stator Blade Wake of an Axial Flow Compressor", *Journal of Engineering for Power*, Oct. 1980, Vol. 102, pp 50-60.
- Ref 6 R. Raj, B. Lakshminarayana, "Characteristics of the wake behind a cascade of airfoils", *Journal of Fluid Mechanics*, vol. 61, part 4, pp. 707-730, 1973.
- Ref 7 John J. Adamczyk, "Aerodynamic analysis of Multistage Turbomachinery Flows in Support of Aerodynamic Design", *Journal of Turbomachinery*, April 2000, Vol. 122, pp 189-217.
- Ref 8 EUREKA: "A Euro-wide Network for Industrial R&D" <http://www.eureka.be/>
- Ref 9 IEC 60193, "Model acceptance tests to determinate the hydraulic performance of hydraulic turbines, storage pumps and pump-turbines", International Standard I.E.C., 1993
- Ref 10 F. Pereira, M. Farhat, F. Avellan, "Dynamic calibration of transient sensors by spark generated cavity". *Proceedings of IUTAM Symposium on Bubble Dynamics and Interface Phenomena*, Birmingham, England, September, 1993.
- Ref 11 TU.Bolleter, "Blade passage tones of centrifugal pump", *Vibration*, Vol. 4, No 3, pp. 8-13.
- Ref 12 C. Nicolet, N. Ruchonnet, F. Avellan "One-Dimensional Modeling of Rotor-stator interaction in Francis Pump-Turbine". *Proceedings of ISROMAC-11, ASME: International Symposium on Transport Phenomena and Dynamics of Rotating Machinery*, Honolulu, Hawaii, USA, February 26-March 2, 2006.
- Ref 13 B. Nennemann, T. Vu, M. Farhat "CFD prediction of unsteady wicket gate-impeller interaction in Francis turbines: A new standard hydraulic design procedure", *Waterpower XIV*, Austin July 18-22, 2005.
- Ref 14 A. Coutu, D. Proulx, S. Coulson, A. Demer "Dynamic Assessment of Hydraulic Turbines", *Hydro Vision 2004*, Montreal, Quebec, Canada, August 16-20, 2004